Available online at www.sciencedirect.com
ScienceDirect
Applied Mathematical Modelling 31 (2007) 934–953
APPLIED MATHEMATICAL MODELLING
www.elsevier.com/locate/apm

Assessment of the effect of high ash content in pulverized coal combustion

S. Jayanti *, K. Maheswaran, V. Saravanan

Department of Chemical Engineering, Indian Institute of Technology, Adyar, Chennai 600 036, India

Received 1 June 2004; received in revised form 1 August 2005; accepted 30 March 2006
Available online 13 June 2006

Abstract

The existing literature on CFD-based coal combustion modelling is applicable mainly for coals of low ash content and the calculations are done on an ash-free basis. In Indian coals, the ash content may be significantly higher, up to 40% or more. Studies reported in the literature show that the mineral matter in the coal may have a number of effects on the combustion characteristics. In the present study, a sensitivity analysis is performed, using the CFD code *CFX* of AEA Technology, on the likely effect of ash content on the char reactivity, oxygen diffusion rate for char combustion and on the radiative heat transfer parameters. The results show that the effect of enhanced char reactivity is negligible whereas reduced oxygen diffusion rates due to a thicker ash layer may result in a significant reduction in char oxidation rates with a resultant decrease in the peak temperature in the furnace. The global parameters such as the peak temperature and the flue gas temperature remain relatively insensitive to the presence of high ash content. These results are consistent with the experimental observations of Kurose et al. [R. Kurose, M. Ikeda, H. Makino, Combustion characteristics of high ash coal in pulverized coal combustion, J. Fuel 80 (2001) 1447–1455].

1. Introduction

There is a vast amount of literature on coal combustion and on the methodologies for the prediction of coal combustion characteristics. Early investigations of coal combustion were mainly based on experimental investigations. Due to the complexity of the phenomena involved in combustion of coal, these were limited initially to simple systems and idealized configurations. The advent of computational fluid dynamics (CFD) has made it possible to investigate the details of complicated flows, especially the relation between flow, turbulence and combustion. CFD-based simulations of coal combustion systems were being reported since the eighties [1–5]. For general reference, the reader is referred to the monograph of Khalil [6] for the overall modelling of combustion processes, to Williams [7] for the combustion theory, to Lawn [8] for the physics of coal combustion,

* Corresponding author. Tel.: +91 4422574168; fax: +91 4422570509.
E-mail address: sjayanti@iitm.ac.in (S. Jayanti).

0307-904X/$ - see front matter © 2006 Elsevier Inc. All rights reserved.
doi:10.1016/j.apm.2006.03.022

to Warnatz et al. [9] for fundamental concepts related to the modelling of coal combustion, and to Ferziger and Peric [10] for general principles of CFD techniques.

The existing literature on coal combustion is mainly applicable for coals of low ash content, typically of the order of 10% by weight. In contrast, Indian coals have relatively less sulphur content but have a high ash content (typically 20–30% but sometimes more than 40% by weight). The ash content also varies significantly from mine to mine from which the coal is extracted. The disposal of fly ash that is produced with high ash coals poses an ecological and environmental problem. Much of the work on high ash coals has been concentrated on the removal methods of ash from the furnace in an eco-friendly manner. However, the effect of high ash content on the performance of the combustor has not been studied systematically.

Some studies reported in the literature show that the nature and amount of ash does affect some of the combustion processes. Sarofim et al. [11] studied the physical transformation of the ash in a pulverized coal under a simulated combustion environment to determine the effect of combustion conditions on the particle size distribution of the ashed mineral constituents produced at combustion temperatures of 1250–1830 K. Three major mechanisms for the particle size distribution were identified: (i) the fusion of the mineral matter finely distributed in the coal matrix and subsequent agglomeration of fused particles on the receding carbon surface; (ii) the formation of cenospheres (due to gas evolution during heating of the minerals) which was found to have a profound effect on the large particle range of the particle size distribution; and (iii) the vaporization and recondensation of particles as sub-micron particles of an increasing percentage of the ash as the combustion temperature increased. The size distribution of the ash particles would have a bearing on the emissivity of the coal combustion products; however, the effect of ash content was not investigated in this study.

Saxena and Rehmat [12] studied theoretically the effect of ash content on coal combustion in a fluidized bed. They showed that the burning time of the coal would increase due to the presence of the ash layer. The combustion rate would be reduced thereby reducing the combustion efficiency. Assuming that the reaction was occurring only at the outer surface of the char particle, Puri [13] modelled the char oxidation with and without the presence of an ash layer. As time progressed, the particle would shrink in size due to radial movement of the reaction front toward the center of the particle and a layer of ash would be formed around the shrinking coal particle (Fig. 1). According to this shrinking core model, for char oxidation to occur in the presence of an ash layer, the oxidant should diffuse through an additional layer of ash to react with the char on its surface. Due to this, the overall diffusion rate of the oxidant to the surface of the char surface would be reduced. The same process is applicable to the product gases evolved from the surface reaction of char. Thus, the char oxidation involves two more processes i.e. diffusion of oxidant through the ash layer and diffusion of reactive products from the reacting surface both of which have a tendency to reduce the combustion rate of char.

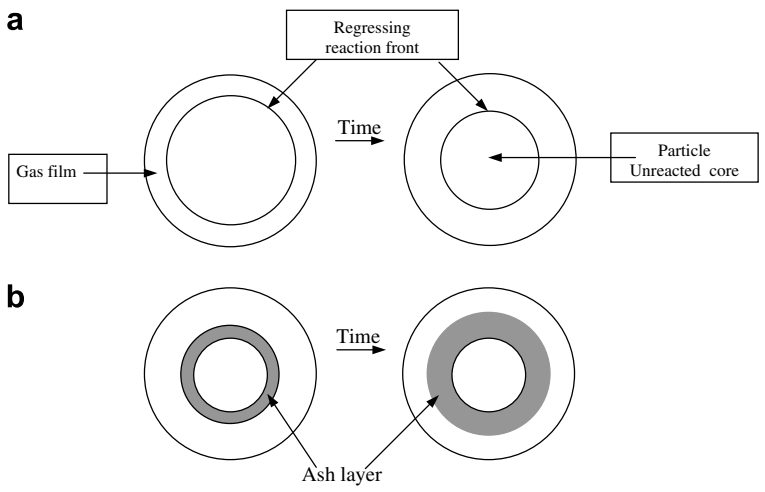

Fig. 1. Shrinking core model (a) without an ash layer, (b) with an ash layer.

Smoot [14] analyzed the effect of the presence of ash and specific minerals in ash can have on the combustion of coal. Several potential effects have been identified; these include:

- Large quantities of ash change the thermal behaviour of particles. Ash consumes energy as it is heated to high temperatures and changes phase.
- Radiative properties of ash differ from those of char and coal and the presence of the ash provides a solid medium for radiative heat transfer when the carbon is consumed.
- Char particles, toward the end of burnout, tend to break into smaller fragments. This breakup process is related to the quantity and nature of the mineral matter in the char.
- Various minerals in the char may have a catalytic effect causing an increase, by up to 30 times, in char reactivity, particularly at low temperatures. However, this effect is likely to be far less prominent at high temperatures.
- Mineral matter provides a barrier through which the reactant, oxygen, must pass to reach the char. Particularly toward the end of burnout, it is possible that high quantities of mineral matter will impede combustion. This can be worsened by softening and melting of the mineral matter.

Apart from the above effects, physical effects of ash such as slagging and fouling on the reactor walls and heat transfer tubes can affect radiative heat transfer and tendency to corrosion.

Recently, Kurose et al. [5] analyzed experimentally the combustion characteristics of high ash coal in pulverized coal combustion. They studied three coals with ash contents of 36%, 44% and 53% by weight and found that the gas temperature and the O_2 concentration at the exit of the furnace were independent of ash content. Under both staged and unstaged combustion conditions, the peak gas temperature decreased as the ash content increased, while the O_2 consumption and NO_x formation and reduction were delayed near the burner. The low combustibility of high ash content case was considered to be caused partly by the large heat capacity of the ash; however, the effect of different specific heats of the ash and the coal particles was found to be negligible.

Thus, it appears that some characteristics of coal combustion are affected by the presence of ash. The extent of the effect would depend on the composition as well as on the amount of ash. Usually such information is not available and a systematic study of the effect of ash content is therefore not possible. In view of this, a sensitivity analysis has been carried out in the present study in which some of the above ash-related effects on combustion parameters are represented by modifying the relevant modelling constants. The calculations are based on the combustion model incorporated in the commercial CFD code *CFX*, version 4.4 developed by AEA Technology, UK. Neglecting the thermal effect associated with the heating of the ash (which has been found to be unimportant by Kurose et al. [5]), the primary parameters studied here are the likely effect on the char reactivity; on the oxygen diffusion to the char particle; and on the emissive characteristics of the media. The details of these calculations and the results obtained are discussed below.

2. Details of the calculation methodology

2.1. Mathematical models

Pulverized coal combustion is a complicated process and its simulation requires a number of models for turbulence, combustion and radiative heat transfer. Each of these requires a considerable simplification of the underlying phenomena and, to a large extent, there is some standardization of the CFD modelling of pulverized coal combustion. The overall calculation process has several elements:

- Flow field calculation for a mixture of gases
- Combustion in two stages: gaseous combustion of volatiles and oxidation of solid char
- Model for turbulence in the gaseous mixture
- Model for turbulence-chemistry interaction during gaseous combustion
- Model for radiative heat transfer
- Models for release of volatile constituents upon heating of coal and for char oxidation

These elements are briefly described below.

2.1.1. Flow field calculation for a mixture of gases

The flow of a Newtonian fluid is given by the continuity and the Navier–Stokes equations. These are valid only for a pure fluid or for a mixture of gases/liquids the composition of which does not change. In a combusting flow situation, the composition of the gaseous mixture changes within the flow domain as the reactants are used up and products are formed. The species conservation equation for such a flow can be derived [15] as

$$\partial/\partial t(\rho_A) + \nabla \cdot (\rho_A \mathbf{u}_A) = S_A, \tag{1}$$

where ρ_A is the density, $\mathbf{u}_A$ is the velocity and S_A is the rate (in kg/m^{3}s) of creation of species A by a source such as a chemical reaction. Defining mass density, mass fraction and mass velocity of the mixture as

$$\text{mass density} = \rho = \Sigma_\alpha \rho_\alpha,$$
$$\text{mass fraction} = Y_\alpha = \rho_\alpha/\rho,$$
$$\text{mass velocity} = \mathbf{u} = \Sigma_\alpha(\rho_\alpha \mathbf{u}_\alpha)/\rho$$

and using Fick's law of diffusion that $\mathbf{J}_A = \rho_A(\mathbf{u}_A - \mathbf{u}) = -\Gamma \nabla Y_A$, where $\mathbf{J}$ is the diffusive flux, one can derive the more useful form of species balance equation in terms of mixture properties:

$$\partial/\partial t(\rho_A) + \nabla \cdot (\rho_A \mathbf{u}) = \nabla \cdot (\Gamma \nabla Y_A) + S_A. \tag{2}$$

Summing over all species, the mixture continuity equation can be written as

$$\partial/\partial t(\rho) + \nabla \cdot (\rho \mathbf{u}) = 0 \text{ as } \Sigma_\alpha \mathbf{J}_\alpha = \Sigma_\alpha S_\alpha = 0. \tag{3}$$

Here $\mathbf{u}$ is the mass velocity. Similarly, the momentum and energy equations can be written for the mixture as

Momentum

$$\partial/\partial t(\rho \mathbf{u}) + \nabla \cdot (\rho \mathbf{u}\mathbf{u}) = -\nabla p + \nabla \cdot \{\mu[\nabla \mathbf{u} + (\nabla \mathbf{u})^{\mathrm{T}}]\}. \tag{4}$$

Energy

$$\partial/\partial t(\rho H) + \nabla \cdot (\rho \mathbf{u} H) = \partial p/\partial t + \nabla \cdot (\lambda \nabla T) + \nabla \cdot \{\mu[\nabla \mathbf{u} + (\nabla \mathbf{u})^{\mathrm{T}}]\}\mathbf{u} + Q_{\mathrm{R}}, \tag{5}$$

where μ and λ are the viscosity and thermal conductivity of the fluid and Q_{R} is the rate of heat release from chemical reaction. The total enthalpy H here is defined as

$$H = h + 1/2\mathbf{u}^2,$$

where h is the static enthalpy and is evaluated in terms of specific heat as

$$h(T) = \int_0^T [C_p(T')]\,\mathrm{d}T' - \int_0^{T_{\mathrm{ref}}} [C_p(T')]\,\mathrm{d}T',$$

where T_{ref} is a reference temperature at which the static enthalpy is taken to be zero. This definition is extended for a mixture of gases also assuming that the constituent species are thermally perfect, i.e., their static enthalpies are functions only of temperature. Thus, the static enthalpy for species A is evaluated as

$$h_A(T) = \langle C_{pA}(T)\rangle T - \langle C_{pB}(T_{\mathrm{ref}})\rangle T_{\mathrm{ref}},$$

where $\langle C_{pA}\rangle$ is the average specific heat and $\langle C_{pB}\rangle$ is the average specific heat of one of the fluid components (for example, the "oxidant" species for combustion). The static enthalpy for the mixture is then given by

$$h(T) = \sum_A \{Y_A h_A\} = \langle C_p(T)\rangle T - \langle C_{pB}(T_{\mathrm{ref}})\rangle T_{\mathrm{ref}},$$

where $\langle C_p\rangle = \sum_A \{Y_A \langle C_{pA}\rangle\}$. For combustion calculations involving hydrocarbons, a simplified chemical reaction framework is employed (see below) and only a limited number of species are used. The average specific heat for these is expressed in terms of a cubic polynomial, the constants, as employed in the computer code *CFX* are given in Table 1.

Table 1
Constants used in the evaluation of the specific heats as $C_P = A_0 + A_1T + A_2T^2 + A_3T^3$

Species	A_0	A_1	A_2	A_3
CH_4	710.7	5.306	−1.742E−3	196.0E−9
C_2H_6	115.7	6.191	−2.609E−3	396.0E−9
C_3H_8	66.78	6.246	−2.776E−3	444.0E−9
C_4H_{10}	108.67	6.117	−2.761E−3	448.0E−9
C_5H_{12}	−35.11	6.676	−3.464E−3	691.3E−9
C_6H_{14}	−38.47	6.681	−3.518E−3	714.3E−9
C_2H_4	1024.7	3.406	−1.294E−3	225.6E−9
C_3H_6	40.51	5.736	−2.931E−3	585.0E−9
C_4H_8	159.37	5.606	−2.816E−3	550.1E−9
H_2	12788.7	2.107	2.178E−4	−144.0E−9
CO	947.9	0.2882	−4.740E−5	−4.0E−9
CO_2	570.8	1.140	−5.700E−4	100.0E−9
N_2	967.3	0.2022	1.518E−5	−17.2E−9
O_2	787.7	0.4884	−2.250E−4	40.0E−9
H_2O	1700.6	0.4428	2.358E−4	−84.2E−9

The evaluation of the rate of creation of species, S_A, and the heat source term Q_R due to chemical reaction can be explained as follows in the context of a generic chemical reaction scheme involving N_S number of species in N_R number of reactions. The jth reaction in this scheme can be written as

$$a_{r1j}X_1 + a_{r2j}X_2 + \cdot + a_{rij}X_i + \cdots \Longleftrightarrow a_{p1j}X_1 + a_{p2j}X_2 + \cdots + a_{pij}X_i + \cdots \quad \text{where } i = 1, 2, \ldots N_S, \tag{6}$$

where a_{rij} and a_{pij} are the stoichiometric coefficients for reactants and products, respectively and $n_{ij} = (a_{pij} - a_{rij})$ is the overall stoichiometric coefficient for species i and in reaction j. The reaction rate R_j for the jth reaction is modeled as a function of the molar concentrations of the reactants and the products as

$$R_j = k_{f_j} \prod_i [X_i]^{\alpha_{ij}} - k_{bj} \prod_i [X_i]^{\beta_{ij}}, \tag{7}$$

where $[X_i]$ is the molar concentration of species i, k_{fj} and k_{bj} are the forward and backward jth reaction rate constants and α_{ij} and β_{ij} are the forward and the backward rate exponents for species i in the jth reaction. The rate constants themselves are evaluated in terms of a modified Arrhenius law involving activation energy, activation temperature and a temperature-dependent pre-exponential factor [16].

With this formulation, the species source term S_A in Eq. (1) can be written for the entire set of chemical reactions as

$$S_A = W_A \Sigma_j (n_{Aj} R_j) \quad j = 1, 2, \ldots, N_R, \tag{8}$$

where W_A is the molecular weight of species A. The source term Q_R due to chemical reaction in the energy Eq. (5) is given in terms of heat of jth reaction (ΔH_{R_j}) as

$$Q_R = -\Sigma_j \{R_j \Delta H_{R_j}(T_{ref})\} \quad j = 1, 2, \ldots, N_R, \tag{9}$$

which can be evaluated in terms of the heat of formation of species at reference temperature T_{refi}, $h_{fi}(T_{refi})$, as

$$Q_R = -\Sigma_j \{R_j [\Sigma_i n_{ij} W_i h_{fi}(T_{refi})]\}. \tag{10}$$

Thus, when dealing with a gas containing a mixture of N_S constituent species, one would solve one mixture continuity, one mixture momentum equation and one energy equation and $(N_S - 1)$ species mass conservation equations. The first two, namely, the continuity and the momentum equation are unchanged except that the properties are defined for a mixture while the energy equation has an additional term arising from heat of reaction.

2.1.2. Combustion modelling

Coal is an inhomogeneous mixture of several organic fuels and inorganic, non-combustible compounds. Its combustion can in principle be represented by a series of chemical reactions. However, combustion of even

light hydrocarbons involves hundreds of chemical reactions and in view of its heterogeneity, pulverized coal combustion is modelled as a two-stage process: in the first stage, volatile fuel (mixture of hydrocarbon gases) is released upon heating of the coal particle which then combusts with the oxygen available in air, and in the second stage, the solid char particle undergoes a slow oxidation in a surface reaction.

2.1.2.1. Gaseous combustion model. The gaseous combustion of volatiles gases is modelled as an irreversible, single-step reaction involving fuel and oxidant as follows:

$$1 \text{ kg of fuel} + i \text{ kg of oxidant} \rightarrow (1+i) \text{ kg of products.} \tag{11}$$

The composition of the fuel, oxidant, combustion products etc in the mixture can be determined from the mixture fraction, f, which couples the mass fractions of the fuel and the oxidant and which is defined as

$$f = \frac{\chi - \chi_o}{\chi_F - \chi_o}, \tag{12}$$

where χ is the Zeldovich variable defined as

$$\chi = Y_F - Y_O/i$$

and Y is the mass fraction and subscripts F and O refer to fuel and oxidant streams respectively. At the inlet to the fuel stream, the oxidant mass fraction is zero and $\chi_F = 1$. Similarly, at the oxidant stream, the fuel mass fraction is zero and hence here $\chi_o = -\frac{1}{i}$. By definition, f is always positive and attains its stoichiometric value $f_{st} = 1/(1+i)$ when $\chi_o = 0$. When $f < f_{st}$, the mixture is fuel deficient and when $f > f_{st}$, it is fuel rich. It can be shown [17] that the mixture fraction obeys the transport equation:

$$\partial/\partial t(\rho f) + \nabla \cdot (\rho \mathbf{u} f) = \nabla \cdot [(\mu/\sigma_L)\nabla f) \tag{13}$$

from which the value of mixture fraction at any location in the flow domain can be computed. To evaluate the individual components of the fuel, the oxidant and the products, an infinitely fast chemical reaction (the "mixed-is-burnt" model) is assumed so that the fuel and the oxidant cannot co-exist simultaneously. The individual mass fractions are then given in terms of the local mixture fraction as

$$Y_F = [f - f_{st}(1 - Y_{pc})]/(1 - f_{st}), Y_O = 0 \quad \text{when } f > f_{st}(1 - Y_{pc}) \tag{14a}$$

and

$$Y_F = 0, \quad Y_O = (1 - Y_{pc} - f/f_{st}) = 0 \quad \text{when } f < f_{st}(1 - Y_{pc}) \tag{14b}$$

where Y_{pc} is the mass fraction of the char products, which is obtained by solving an extra scalar equation with the source term arising from the char oxidation model (see Section 2.1.2.3).

2.1.2.2. Devolatilization model. When a coal particle is subjected to intense heating, the volatile components first evolve from the particle, and then subsequently burn into gas phase. This process, the evolution of volatile gases from the coal, is termed as devolatilization. The volatile matter is released from a temperature of about 800 K [18]. The characteristic time of release of volatiles from a coal particle is 30 ms. In the present study, the devolatilization is modelled as a single reaction of Badzioch and Hawksley [19]. In this model, the coal is considered to have fixed fractions of volatiles, char and ash. The rate of production of the volatile gases is given by the first order reaction

$$\frac{dV}{dt} = k_v(V_f - V), \tag{15a}$$

where V is the mass of volatiles which have already evolved from unit mass of raw coal, and V_f is the final yield of volatiles. The rate constant k_v is expressed in Arrhenius form as

$$k_v = A_v \exp\left(-\frac{E_v}{T_p}\right), \tag{15b}$$

where T_p is the temperature of coal particle (assumed to be uniform), and A_v and E_v are constants, determined experimentally for a particular coal. While V_f is required as input data, the temperature of the coal particle is obtained through a Lagrangian particle trajectory calculation (see Section 2.1.3).

2.1.2.3. Char oxidation model. The second stage of coal combustion following the devolatilization is the char combustion. Char combustion is much slower process than devolatilization, and therefore it determines the burning rate of the pulverized coal in the furnaces. In the present study, char combustion is calculated using the model of Field et al. [20] which is based on classical shrinking core model [13]. In this model, a char particle is considered to be a spherical particle surrounded by a stagnant boundary layer through which oxygen must diffuse before it reacts with the char. The oxidation is assumed to be limited by the diffusion of oxygen to the external surface of the char particle and by the effective char reactivity. The rate of diffusion of oxygen is given by $k_d(P_g - P_s)$, where P_g is the partial pressure of oxygen in the furnace gases far from the particle boundary layer and P_s is the oxygen pressure at the particle surface. The value of k_d is given by

$$k_d = \frac{2.53 \times 10^{-7}}{R_p}\left(\frac{T_p + T_g}{2}\right)^{0.75}\frac{P_A}{P}, \tag{16a}$$

where R_p is the radius of the coal particle, T_g is the far-field gas temperature in the furnace, P is the local pressure and P_A is atmospheric pressure. The char oxidation rate unit area of the particle as a first order reaction is given by $k_c P_s$, where k_c is the chemical rate coefficient, which is given by

$$k_c = A_c T_p \exp\left(-\frac{T_c}{T_p}\right), \tag{16b}$$

where A_c and T_c are the Arrhenius constants the values of which depend on the type of the coal and specified as input parameters in the calculations. The overall char reaction rate of a coal particle is given by

$$(k_c^{-1} + k_d^{-1})^{-1} P_g 4\pi R_p^2 \frac{P}{P_A} \tag{17}$$

and is controlled by the smaller of the rates k_d and k_c. The constants appearing in this model are listed in Table 2.

2.1.3. Particle tracking and coupling

The combustion of the coal particle is calculated by simulating the coal particle motion in a Lagrangian frame of reference. The velocity of spherical coal particles of given initial mass, composition, temperature and velocity are computed by integrating the momentum balance on the particle subject to inertial, drag, grav-

Table 2
Constants used in the mathematical model

Constant	Equation in which it appears	Value of the constant
A_c (kg/m^2/atm/s)	16b	497
A_v (kg/m^2/atm/s)	15b	1,34,000
c_1	25	1.44
c_2	25	1.92
c_μ	23	0.09
c_{g1}	31	2.22
c_{g2}	31	2.0
E_v (K)	15b	74,000
T_c (K)	16b	8540
V_f	15a	0.529
σ_f	30	0.9
σ_g	31	2.0
σ_ε	24	1.0
σ_Y	27	0.9
σ_ε	25	1.22

itational and other forces. The position of the particle is then obtained by integrating the velocity of the particle. The heating up of the particle is considered through an empirical correlation for convective heat transfer and a particle emissivity factor for the radiative pre-heating of the particle. Terms relating to momentum and heat transfer associated with mass transfer are also included. The trajectory equations, and the auxiliary equations describing heat or mass transfer to/from the particle, are solved by stepwise integration over discrete time steps. Along the trajectory of a particle, there is exchange of heat, mass, and momentum between the particle gained or lost by the particle stream that follows that trajectory and these quantities can be incorporated in the subsequent continuous phase calculations. This two-way coupling is accomplished by alternately solving the discrete and the continuous phase equations until the solutions in both phases have stopped changing.

2.1.4. Radiative heat transfer

In a combusting environment, radiative heat transfer is the dominant mode of heat transfer. It is governed by the radiative transfer equation (RTE) which for an absorbing, emitting and scattering medium at position $\boldsymbol{r}$ in the direction $\boldsymbol{s}$ is given by

$$\frac{\mathrm{d}I(r,s)}{\mathrm{d}s} + (a+\sigma_\mathrm{s})I(r,s) = an^2\frac{\sigma T^4}{\pi} + \frac{\sigma_\mathrm{s}}{4\pi}\int_0^{4\pi} I(r,s)\Phi(s\cdot s')\,\mathrm{d}\Omega', \tag{18}$$

where $\boldsymbol{s}'$ is the scattering direction vector, s is the path length, a is the absorptivity, n is the refractive index, σ_s is the scattering coefficient, σ is the Stefan–Boltzman constant, I is total radiation intensity, T is the local temperature, Φ is the phase function and Ω' is the solid angle. The solution of above integro-differential equation is very complex and consumes enormous computational time. Several approximate methods have been developed to deal with radiative heat transfer in practical combusting systems; these have been reviewed in detail by Viskanta and Menguc [21]. In the present study, the discrete transfer radiation model (DTRM) is used. The main approximation in this model is that the radiation leaving the surface element in a certain range of solid angles can be approximated by a single ray. Assuming diffuse surfaces, grey gas radiation and the scattering to be negligible, the equation for the change of intensity of radiation, dI, along a path, ds, can be written as

$$\frac{\mathrm{d}I}{\mathrm{d}s} + aI = \frac{a\sigma T^4}{\pi}. \tag{19}$$

The DTRM integrates Eq. (19) along a series of rays emanating from a boundary faces. If a is constant along the ray, then $I(s)$ can be estimated as

$$I(s) = \frac{\sigma T^4}{\pi}(1-\exp[-as]) + I_0\exp[-as], \tag{20}$$

where I_o is the radiant intensity at the start of the incremental path, which is determined by the appropriate boundary condition. The energy source in the fluid due to radiation is then computed by summing the change in intensity along the path of each ray that is traced through the fluid control volume. The ray tracing technique used in the DTRM can provide a prediction of radiation heat transfer between surfaces without explicit view factor calculations. The accuracy of the model is limited mainly by the number of rays traced and the computational grid.

2.1.5. Turbulence effects

In turbulent flow, the flow variables, namely, velocity, pressure, enthalpy (or temperature) and species mass fractions, fluctuate in time in such a way that higher rates of diffusivity of mass, momentum and heat occur. Trying to do reproduce all the typical fine scale turbulent fluctuations is possible through the solution of the time-dependent form of the governing equations (''direct numerical simulation''—DNS—of turbulence) but is practically impossible. The usual approach is to solve the Reynolds-(time-) averaged Navier–Stokes (RANS) equations:

$$\frac{\partial\overline{U}_i}{\partial t} + \frac{\partial(\overline{U}_i\overline{U}_j)}{\partial x_j} = -\frac{1}{\rho}\frac{\partial\overline{P}}{\partial x_i} + \frac{\partial}{\partial x_j}\left[\nu\left(\frac{\partial\overline{U}_i}{\partial x_j} - \overline{u_i'u_j'}\right)\right], \tag{21}$$

where an overbar indicates the time-averaged component and a prime denotes the fluctuating component of a variable. As can be seen, the time-averaging of the momentum equations results in the appearance of the extra terms ($\overline{u_i'u_j'}$ or "Reynolds stresses" in Eq. (21)) leading to the closure problem of turbulence [22]. A number of phenomenological models have been developed therefore to calculate the single-phase flow field under turbulent conditions; the one used in the present study is the $k-\varepsilon$ model in which the Reynolds stresses are evaluated using the Boussinesq hypothesis:

$$\overline{u_i'u_i'} = -v_t\left(\frac{\partial \overline{U}_i}{\partial x_j} + \frac{\partial \overline{U}_j}{\partial x_i}\right) + \frac{2}{3}k\delta_{ij}, \tag{22}$$

where v_t, the turbulent or eddy viscosity, is expressed in terms of two variables characterizing local turbulence, namely, the turbulent kinetic energy, $k = 1/2\overline{u_i'u_j'}$ and the rate of dissipation of turbulent kinetic energy, $\varepsilon = v\overline{\frac{\partial u_i'}{\partial x_j}\frac{\partial u_i'}{\partial x_j}}$, as

$$\mu_t = \rho v_t = \rho c_\mu \frac{k^2}{\varepsilon}. \tag{23}$$

Exact transport equations for k and ε can be derived [22]; however, many more variables are introduced in the process and several approximations have to be made. The final "modeled" form of the k- and ε- equations are as follows:

$$\frac{\partial k}{\partial t} + \frac{\partial (k\overline{U}_j)}{\partial x_j} = v_t\left(\frac{\partial \overline{U}_i}{\partial x_j} + \frac{\partial \overline{U}_j}{\partial x_i}\right)\frac{\partial \overline{U}_i}{\partial x_j} + \frac{\partial}{\partial x_j}\left(\frac{v_t}{\sigma_k}\frac{\partial k}{\partial x_j}\right) - \varepsilon, \tag{24}$$

$$\frac{\partial \varepsilon}{\partial t} + \frac{\partial (\varepsilon\overline{U}_j)}{\partial x_j} = c_1\frac{\varepsilon}{k}v_t\left(\frac{\partial \overline{U}_i}{\partial x_j} + \frac{\partial \overline{U}_j}{\partial x_i}\right)\frac{\partial \overline{U}_i}{\partial x_j} + \frac{\partial}{\partial x_j}\left(\frac{v_t}{\sigma_k}\frac{\partial \varepsilon}{\partial x_j}\right) - c_2\frac{\varepsilon^2}{k}, \tag{25}$$

where the values of the constants are given in Table 2.

Thus, for turbulent flow, one has to solve the time-averaged, modeled form of continuity and momentum equations along with the transport equations for k and ε. For combusting flows, the energy conservation equation and the mixture fraction equation have to be similarly time-averaged and modeled. The final form of these equations is as follows:

Time-averaged energy conservation equation:

$$\frac{\partial \rho\overline{H}}{\partial t} + \nabla\cdot(\rho\overline{UH} + \rho\overline{u'h'}) = \frac{\partial p}{\partial t} + \lambda\nabla\overline{T}. \tag{26}$$

Time-averaged mixture fraction equation:

$$\frac{\partial \rho\overline{Y}_A}{\partial t} + \nabla\cdot(\rho\overline{UY}_A + \rho\overline{u'Y_{A'}}) = \nabla\cdot\left(\frac{\mu_t}{\sigma_Y}\nabla\overline{Y}_A\right) + \overline{S}_A. \tag{27}$$

For combusting flows involving chemical reactions, estimation of the reaction using time-averaged concentrations can lead to erroneous results as at any point the mixture may be composed of fuel and products at one instant and of oxidant and products at a different time. Thus, the mean fuel and oxidant concentration profiles have considerable overlap in the region where the reaction is taking place. Also, estimation of the reaction rate constant based on the mean temperature when the rate is a highly non-linear function of temperature can also be inadequate. One approach to modelling concentration fluctuations (see, for example [9]) is to take a single conserved scalar quantity, such as the mixture fraction, and to model the fluctuations of this quantity, i.e., to specify the statistics of the fluctuations, by introducing a probability distribution function, $p(f)$, such that $0 \leqslant p(f)$ and $\int_0^1 p(f)\,\mathrm{d}f = 1$. The time average of any variable ξ, such as $m_{F,}$ which is a function of f, is then given by

$$\bar{\xi} = \int_0^1 \xi f p(f)\,\mathrm{d}f. \tag{28}$$

Several models of $p(f)$, such as the double delta function, the beta function and the clipped Gaussian function, can be used. In the present study, the $p(f)$ is modeled using a double delta function. The formulation of the double delta function is given below:

$$p(f) = A\delta(f - \bar{f}_+) + B\delta(f - \bar{f}_-) \quad \text{with } \bar{f}_+ = \bar{f} + \alpha, \bar{f}_- = \bar{f} - \alpha, \tag{29}$$

where $\bar{f}$ is the time-averaged mixture fraction. This model contains three constants *A, B,* α *which* are determined from the conditions that the distribution functions must satisfy the normalization integral, give the correct mean of f and the correct mean square of f. The mean and mean square values of f, $\bar{f}$ and G, respectively, are then calculated from the transport equations:

$$\frac{\partial \rho u \bar{f}}{\partial t} + \nabla \cdot (\rho \overline{U} \bar{f}) - \nabla \cdot \left(\left(\frac{\mu_t}{\sigma_f} + \frac{\mu}{\sigma_L} \right) \nabla \bar{f} \right) = 0, \tag{30}$$

$$\frac{\partial \rho G}{\partial t} + \nabla \cdot (\rho \overline{U} G) - \nabla \cdot \left(\left(\frac{\mu_t}{\sigma_g} + \frac{\mu}{\sigma_L} \right) \nabla G \right) = C_{g1} \mu_t (\nabla \bar{f})^2 - C_{g2} \rho \frac{\varepsilon}{k} G. \tag{31}$$

Here, C_{g1} and C_{g2} are model constants and σ_f and σ_g are the equivalent turbulent Prandtl numbers. The values of these parameters are given in Table 2.

The mean mass fractions of the fuel, oxidant and products are then obtained from

$$\overline{Y_F} = \int_0^1 \max \left(\frac{\bar{f} - f_{st}(1 - \overline{Y_{pc}})}{1 - f_{st}}, 0 \right) p(f)\, df,$$

$$\overline{Y_O} = \int_0^1 \max \left(1 - \overline{Y_{pc}} - \frac{\bar{f}}{f_{st}}, 0 \right) p(f)\, df$$

and

$$\overline{Y_p} = 1 - \overline{Y_F} - \overline{Y_O} - \overline{Y_{pc}}.$$

Finally, turbulence in the continuous phase also has an effect on the motion of the coal particles. The turbulent dispersion of these particles is determined using a stochastic approach based on the model of Hutchinson et al. [23] wherein the particle is assumed to interact with a series of randomly oriented, randomly sized eddies of randomly distributed lifetimes expressed in terms of the local turbulent kinetic energy and its dissipation rate.

2.2. Numerical details

2.2.1. Geometrical details

The geometry of the furnace used in the present calculations is IFRF No. 1 furnace and is shown schematically in Fig. 2. It essentially consists of a co-axial burner with the radius at the throat of the divergent conical quarl (R_s) of 0.304 m. The annular section in the co-axial burner is termed as the secondary section and the inner core part (which is partly blocked by the coal gun) is termed as the primary section. The ratio of the primary to the secondary nozzle radii (R_p/R_s) is 0.6 and the quarl expansion ratio (B/R_s) is 2.0. The ratio of length of the quarl to the diameter of the burner (L/R_s) is 1.0. These correspond to the geometric details

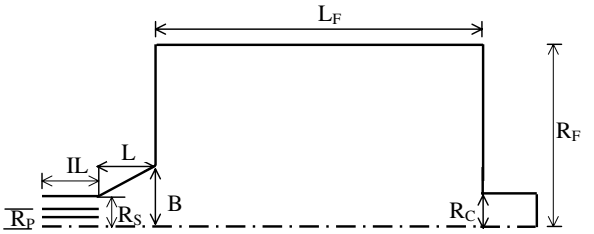

Fig. 2. Typical computational domain used in the present combustion study. $R_s = 152$; $R_p/R_s = 0.6$; $L = 152$; $R_F = 1130$; $B/R_s = 2.0$; $IL = 150$; $R_c = 285$; $L_F = 6250$. All dimensions are in millimeters.

Table 3
Inlet conditions used in the computations

Inlet	Axial velocity (m/s)	Tangential velocity (m/s)	Turbulent kinetic energy (m^2/s^2)	Turbulent dissipation rate (m^2/s^3)	Temperature (K)
Primary air	14.6	0	5.7	365	343
Secondary air	36.5	46.1	31.9	3700	573

of the IFRF Furnace No. 1 [3,4]. The furnace is 6.25 m long with a roughly square cross-section with an arching roof. It is modelled in the present case (as done by [3] as a cylinder with an internal diameter of 2.26 m. The diameter of the outlet contraction is 0.57 m. The beginning of the computational domain is positioned at 0.15 m upstream of the beginning of the quarl expansion. To reduce the number of grids required to model the geometry, the flow is considered to be axisymmetric which renders the problem two-dimensional. The domain is discretized using structured, non-uniform cells, with a grid density of 138×85 in the axial and radial directions, respectively.

2.2.2. Boundary conditions

The pulverized coal along with the transportation air is supplied through the primary section whereas the swirling combustion air is supplied though the secondary inlet. According to the conditions investigated by Visser et al. [3] and Weber et al. [4], the flow rate of transportation air is 0.129 kg/s, the flow rate of combustion air is 0.98 kg/s and the flow rate of coal is 0.124 kg/s. The other inlet conditions for the flow in the primary and secondary inlet are given in the Table 3. The furnace walls are considered to be isothermal walls with a temperature at 400 K and an emissivity of 0.2, while all the other walls including the burner walls are considered to be adiabatic. The total thermal output of the furnace is 3.4 MW according to Visser. However, an exact matching between the present calculations and the experimental and simulation work of Visser, which are also reported in Weber et al., could not be achieved because there was some internal inconsistency in the boundary conditions employed by Visser. The wall boundary conditions have also not been mentioned. Also, the evaluation of the gas temperature is significantly different from that used in CFX (which is enough to cause a deviation of 100 K at typical furnace temperatures). Hence, a one-to-one comparison with the results of Visser et al. [3] is not possible. However, the conditions generated in the reference case are expected to be somewhat similar to those studied by Visser.

2.2.3. Solution procedure

The overall calculation procedure is as follows. The three time-averaged conservation equations, namely, those of mass, momentum and energy, are supplemented by the $k-\varepsilon$ turbulence model to deal with turbulence effects in the gas-phase field. Radiative heat transfer is calculated using a discrete transfer radiation model (DTRM). The trajectories of individual coal particles of given initial size (60 μm) are calculated using a particle tracking model. The coal combustion itself is calculated in three parts: a single-step reaction model for devolatilization; an infinite-rate, single-step, irreversible reaction (the ''mixed-is-burnt'' model) for gaseous combustion; and a shrinking core model for char combustion. The coupling in terms of momentum, heat and mass transfer between the coal particles and the gas phase is taken into account using an Eulerian–Lagrangian framework of calculation. After every 100 iterations of the gas-phase, one set of trajectory calculations is made to determine the coupling between the two phases. This process is repeated 40 times so as to reach a converged solution. The composition of the pulverized coal and the properties of the coal are given in the Table 4. All the calculations were carried out using the commercial CFD code *CFX 4.4*.

3. Results

3.1. Typical results

Typical velocity and the temperature fields obtained in the present study for the reference case with 10.8% by weight of ash are shown in Fig. 3a and b in the form of equi-spaced velocity and temperature contours,

Table 4
Composition and properties of coal used in the present study

Properties of coal	Values
Proximate analysis (% w/w dry basis)	
Volatile matter (%)	36.3
Char (%)	52.9
Ash (%)	10.8
Ultimate analysis (% w/w dry ash free basis)	
Carbon (%)	75.37
Hydrogen (%)	4.47
Nitrogen (%)	1.15
Oxygen (%)	18.94
Properties of coal	
Particle size (μm)	60
Density of char (kg/m^3)	2000
Density of volatiles (kg/m^3)	1560
Density of ash (kg/m^3)	1000
LCV of volatiles (MJ/kg)	2.623
LCV of char (MJ/kg)	3.29
Molecular weight of coal	93
Emissivity of coal	1.0
Emissivity of char	0.6
Mass flow rate (kg/s)	0.124

respectively. The velocity associated with the annular secondary air jet is the highest and due to the strong swirl (the swirl number being 0.62), the jet is deflected away from the centre and the flow follows the contour of the conical quarl wall. This sets up an inner recirculation zone, which brings back the hot gases and aids in combustion. The shape of the quarl is therefore expected to play a significant role in defining the extent of the IRZ. The temperature contours show that high gas temperatures are found slightly beyond the quarl region. They also clearly show the hot zone close to the burner inlet created by the recirculation of the hot gases.

For this case, the total thermal output is predicted to be 3.275 MW which compares well with the expected value of 3.4 MW quoted by Visser et al. [3] and the value of 3.34 MW expected from the calorific value and the amount of fuel added. The simulations show that the fuel is completely burnt. The maximum and the outlet gas temperature predicted for this case are 1956 K and 1060 K, respectively, which show a larger deviation from the simulations of Visser, who found the corresponding temperatures to be 1880 K and 1420 K. The experimental flue gas temperature was found to be 1320 K. The calculation of the peak gas temperature is principally affected by the correlation for the gas specific heat. Visser used a linear correlation for the specific heat of the gas with temperature while the one used in CFX is a cubic polynomial. It is estimated that this itself might have caused a deviation of up to 100 K in the gas temperature calculation at the peak temperature level. The flue gas temperature is strongly influenced by the thermal boundary conditions as about 70% of the heat

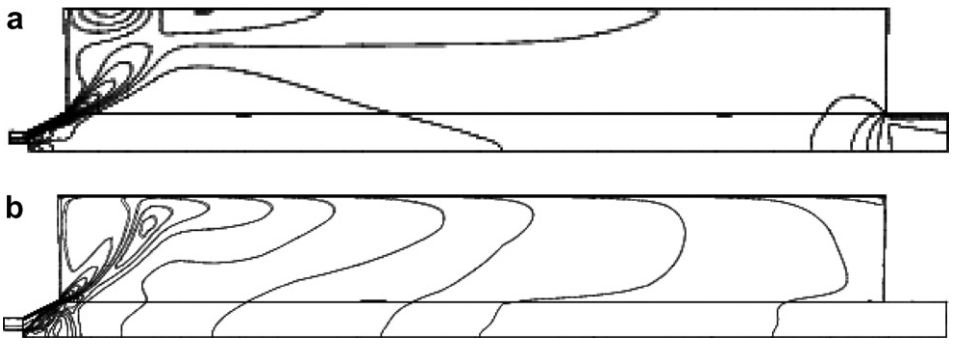

Fig. 3. Equi-spaced velocity (a) and temperature (b) contours for the reference case.

produced is lost through the furnace walls. The thermal boundary conditions in the experiments as well as in the simulations of Visser are not known exactly and this may have caused the larger discrepancy for the flue gas temperature between the present calculations and the simulations of Visser et al. [3]. The purpose of the present study is not to reproduce the data but to investigate the effect of high ash content on combustion. It is felt that the conditions predicted in the present simulations are fairly typical of those encountered in pulverized coal furnaces and that this case can therefore be used as a reference case for the investigation of the effect of ash content.

The Lagrangian tracking of the coal particles enables a detailed investigation of the combustion-related processes taking place inside the furnace. Typical tracks of coal particles, of a size of 60 μm each, introduced in all the cells of the primary inlet are shown in Fig. 4a. It can be seen that all the particles follow a similar path along the furnace walls and they remain nearly as a bunch. The effect of initial particle position was studied in Fig. 4a by comparing the trajectories of two coal particles, one of which is released close to the coal gun and the other close to the divider plate between the primary and the secondary stream, while maintaining all the other characteristics the same. It was found that the trajectories were nearly identical. The path of a single particle through the domain is shown in Fig. 4b where the axial location of the particle is plotted as a function of time. Also marked in this is the location of the quarl section. It can be seen that the total residence time of the coal particle in the furnace is about 3.1 s of which only 17 ms is spent in the quarl region.

The variation of the particle temperature, mass of the volatiles left in the particle and the mass of the char left in the particle for a typical particle are shown in Fig. 5a as a function of axial position and in Fig. 5b as a function of residence time. The particle goes through an initial phase of rapid heating and attains a peak temperature of nearly 2400 K before cooling off. The sensible heating part lasts about 25 ms during which their temperature rises from 343 K to 773 K. This gives a heating rate of 1.7×10^4 K/s which is in agreement with the typical range of heating rates (10^4–10^5 K/s) reported by Wall [18] for pulverized coal combustion. It is expected (Visser, 1991) that for this coal, the devolatilization starts at 773 K and is over at temperature of

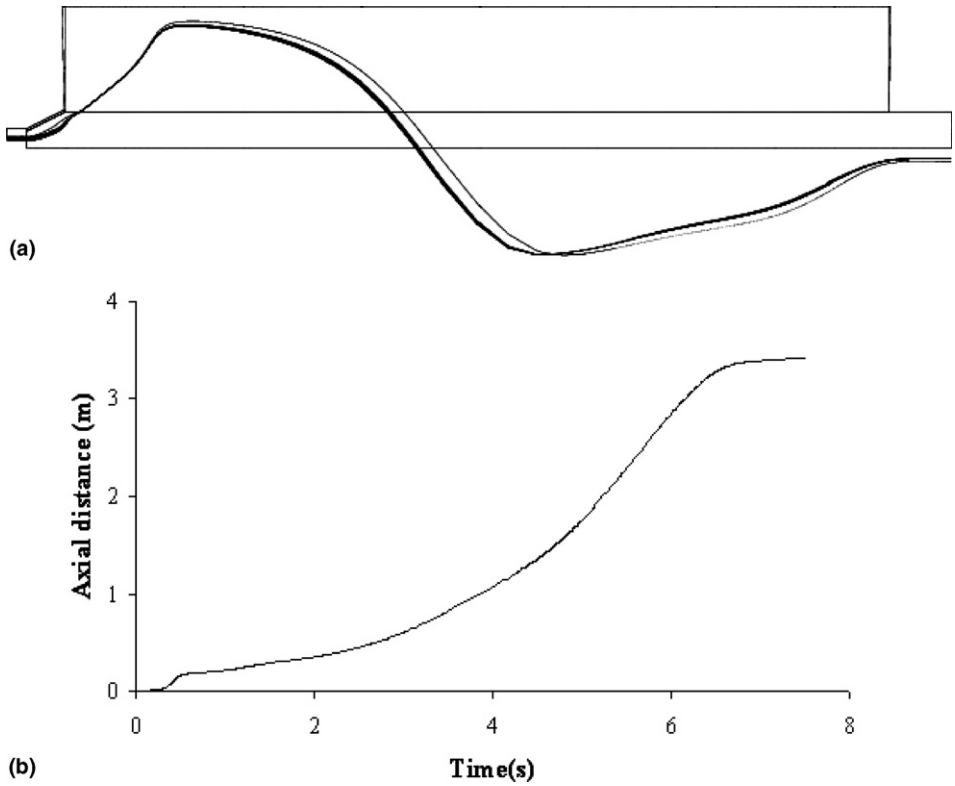

Fig. 4. (a) Trajectories of 60 μm particles and (b) variation of axial distance with time.

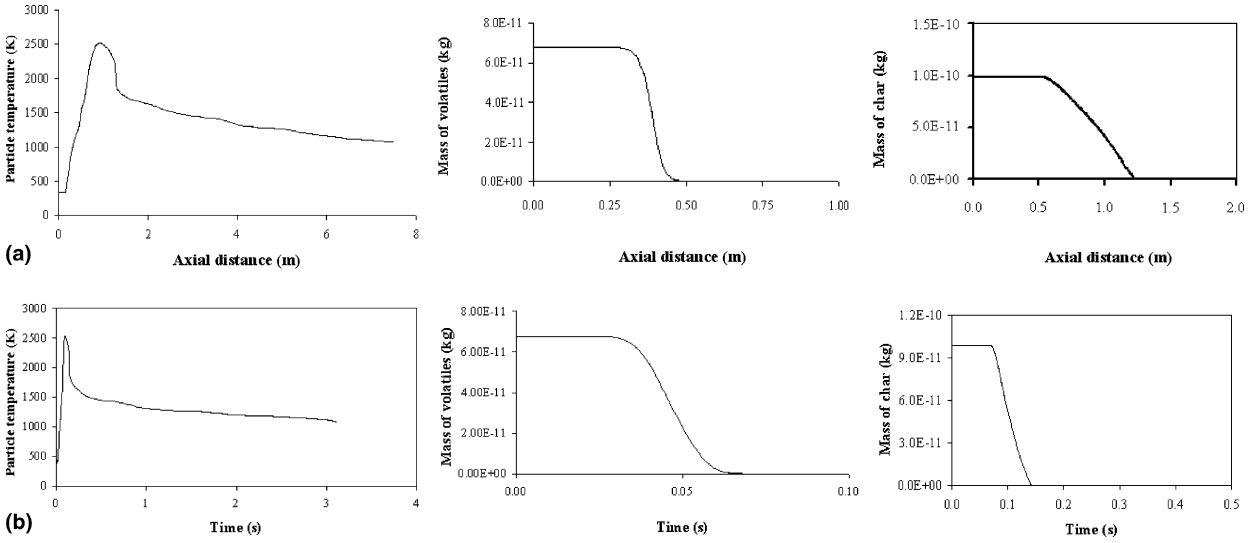

Fig. 5. Variation with (a) axial position and (b) time of (i) particle temperature variation, (ii) mass of volatiles left, and (iii) mass of char left unburnt for the reference case.

1243 K. The particle takes a further time of about 40 ms to reach a temperature of reaches a temperature of 1253 K. Thus, the devolatilization is completed within 65 ms of entering the furnace. The variation of the mass of volatiles and the mass of char in the coal particle shows that, in terms of distance, devolatilization starts halfway through the quarl and is completed over the next 0.15 m. The next stage of the coal combustion, char combustion starts after 65 ms at a temperature of around 1300 K at a distance of about 0.5 m from the inlet and extends up to 1.25 m downstream. Thus, the entire combustion process is over within 150 ms and around 1.25 m from the inlet of the domain. This explains the location of the temperature maximum at some distance from the quarl as the heat release associated with char combustion happens outside the quarl region.

An analysis of the thermal balance of the furnace shows that amount of heat transferred through the walls (with a wall temperature of 400 K and a uniform emissivity of 0.2) is 2.364 MW and through outlet of the furnace is 1.597 MW. Thus, more heat is transferred through the walls of the furnace rather than through the outlet. Since the furnace is 6.25 m long, a large area is available for heat transfer. Visser et al. [3] used an adiabatic boundary condition for the furnace walls except at the locations of cooling loops. This could lead to a lesser amount of heat transfer through the walls in his case compared with the present study and may thus explain the significantly higher gas outlet temperature of 1420 K obtained by him compared to that of 1060 in the present case.

The above results are taken as the reference case for a "low-ash" coal, in this case, an ash content of 10.8% by weight, and the effect of increased ash content on these combustion parameters is studied by modifying the model constants in a manner consistent with the expected influence of ash. The results are discussed below.

3.2. Momentum and heat transfer coupling between gas and coal particles

One important aspect of coal combustion is the momentum and heat transfer coupling between the gas and coal particles. The coal particles are obviously influenced by the gas flow in terms of their trajectory as well as in terms of radiative heating and more indirectly in terms of oxygen diffusion in the char combustion process. The gas phase is influenced strongly by the heat release as a result of combustion. Thus, there is a two-way coupling between the particulate and the continuous phases. This coupling is taken into account in the calculations by iterative calculation of the coupling terms. Since the effect of ash on combustion is not directly taken into account in the combustion calculation methodology (the calculations are effectively done on an ash-free basis), it is interesting to see how strongly this coupling is affected by the ash content. To this end, calculations have been done with ash content of 20%, 30% and 40% by weight with and without adjusting the coal flow

Table 5
Peak temperature and outlet temperature of the gas, and expected and predicted thermal output for different ash percentages for constant coal flow rate of 0.124 kg/s

Percentage of ash by weight	Peak gas temperature (K)	Outlet gas temperature (K)	Thermal output expected from calorific value (MW)	Thermal output predicted from calculations (MW)
10.8% (Reference case)	1956	1060	3.34	3.275
20%	1903	1025	2.99	2.93
30%	1876	985	2.62	2.54
40%	1849	943	2.2	2.24

rates to maintain the same thermal input to the furnace. None of the modelling constants have been changed in these calculations. If the coupling between the two phases was strong, then one would expect the results to show a consistent variation with the ash content.

Treating the case with the same coal flow rate first, it was found that the predicted temperature contours obtained for the reference case (10.8% ash) and for the cases with 20%, 30% and 40% by weight of ash for the same coal flow rate of 0.124 kg/s did not show much difference. As expected, the overall thermal output decreases when the ash content increases. The comparison of the peak temperature, the flue gas temperature, the predicted and expected thermal load in each case are listed in Table 5. It can be seen that thermal load decreases by about 33% for the maximum ash content of 40%. However, the peak temperature decreases only by about 100 K compared with the reference case. The outlet temperature also decreases consistently with increasing ash content, but again the decrease is rather small, and is of the order of 110 K. These results show that these two temperatures are determined by the extent of heat loss through the walls rather than by the amount of heat generated as a result of combustion. Radiative heat transfer, which is the dominant mode of heat transfer accounting for 80% of heat transfer through the walls, prevents the temperatures from becoming too high since it is proportional to T^4.

The variation of particle temperature, mass of volatiles left and mass of char unburnt as a function of time and axial position are shown in Fig. 6. The effect of increasing ash content is to reduce the mass of volatiles and char. In the present study, as the ash content is increased, these two are reduced in such a way that the C/H ratio remains the same as in the reference case. It can be seen from Fig. 6a that the particle temperature rises faster with increasing ash content. This increases the rate of release of volatiles and the rate of char

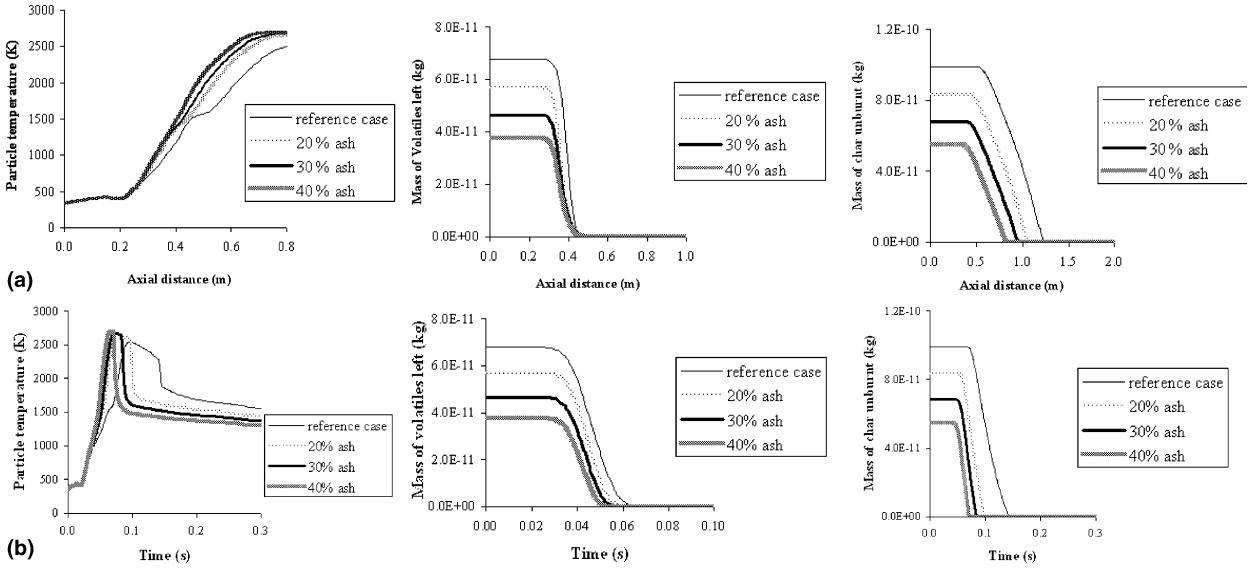

Fig. 6. Variation with (a) axial position and (b) time of (i) particle temperature variation, (ii) mass of volatiles left, and (iii) mass of char left unburnt for different ash contents at the same coal flow rate.

Table 6
Peak temperature and outlet temperature of the gas, and expected and predicted thermal output for different ash percentages for constant thermal load

Percentage of ash by weight	Peak gas temperature (K)	Outlet gas temperature (K)	Thermal output expected from calorific value (MW)	Thermal output predicted from calculations (MW)
10.8% (Reference case)	1956	1060	3.34	3.275
20%	1962	1062	3.4	3.3
30%	1954	1060	3.4	3.26
40%	1945	1059	3.4	3.23

combustion resulting in earlier combustion as the ash content increases. However, the differences are rather small as complete combustion takes place within a short distance from the quarl, as noted earlier. Further variation of the particle temperature is affected by the prevailing gas temperature, and since this is lower at higher ash contents, the particle exit temperature also decreases with increasing ash content. Thus, the combustion rate is affected by the ash content, but the overall effect is small.

The results obtained with the cases where the overall thermal load is maintained constant is summarized in Table 6. Here, the flow rate of coal is increased to compensate for the loss in calorific value as the ash content is increased. The predicted peak and flue gas temperatures are hardly changed by these significant changes in the ash content and the corresponding changes in the coal flow rate. Similarly, the variation of the coal particle characteristics with distance and time for these cases was found to be nearly identical in the latter part of the furnace; however, very near the quarl, some effect of the ash content was noticed. Taken together, these results show that the temperature history of the particle is governed mainly by combustion (both volatiles and char) in the near-burner region and by convective and radiative heat transfer in the rest of the furnace. If the thermal output is maintained the same, the ash content does not have much influence, through the momentum and heat transfer coupling, on the combustion characteristics. The influence through other mechanisms is discussed below.

3.3. Effect on char reactivity

As discussed in Section 2.1.2.3, char combustion is a much slower process than devolatilization and it therefore determines the burn-out time of the coal in the furnace. In the present calculations, the model of Field et al. [20] is used to describe char combustion. The overall oxidation rate of the char is calculated by the diffusion of oxygen to the external surface of the char particle and the effective char reactivity and is given by Eq. (17) where the oxygen diffusion rate and the char reactivity are given, respectively, by Eqs. (16a) and (16b). Sarofim et al. [11] found that the mineral matter enhances the char reactivity during coal combustion by up to a factor of 30 although the increase is less at high temperatures. Assuming that increased ash content (ash being mineral matter) would increase the char reactivity, calculations have been done by increasing the constant A_c in Eq. (16b) from 490 to 5000, i.e., by a factor of ten. This would have the effect of increasing the chemical rate of char reactivity by a factor of ten. Comparison of the predicted axial variation of temperature, mass of volatiles and mass of char with those of the reference case showed that the change had very little effect on the mass of volatiles while the rate of char combustion was increased slightly and correspondingly the temperature rise in the near-burner region was faster. However, since the overall thermal load was constant, the temperature variation further downstream was not affected significantly.

An estimate of the likely effect of enhanced char reactivity can be made. The overall char reaction is governed by k_c and k_d which are the chemical rate and the rate determined by oxygen diffusion, respectively. For a typical coal combustion calculations in the reference case, at a distance of 0.50 m from the computational inlet where char combustion begins, the particle temperature is 1790 K, the gas temperature 1500 K, and with the particle diameter of 60 μm, the values of k_c and k_d are found to be 6607 kg/m^2/atm/s and 2.15 kg/m^2/atm/s, respectively. This shows that the effect of char reactivity would only be slight. However, at lower temperatures, i.e., in the initial phases of combustion, k_c is expected to be smaller and the chemical rate may be the

determining process. Hence, increasing it by a factor 10, as done in the present case would increase the rate of char combustion in the initial phases. This was found to be the case although the effect of this on the overall char combustion was rather limited as the char combustion in the reference case itself (with lower reactivity) is completed within a very short distance from the quarl.

3.4. Effect of ash on oxygen diffusion rate

In the classical shrinking core model of char combustion, the effect of ash is taken into account by considering a thin ash layer surrounding the char particle through which oxygen has to diffuse. Accordingly, the diffusion rate of oxygen is reduced in the presence of ash [13]. If the ash content increases significantly, it is possible that the thickness of the hypothetical ash layer surrounding the char particle may also increase. This would have the effect of further decreasing the rate of diffusion of oxygen to the surface of the combusting char particle. Thus, k_d will be reduced as the ash content of the coal increases.

In order to see if this would have a significant effect on the overall furnace parameters, calculations would have to be made with reduced values of k_d. This can be done for example by reducing the coefficient 2.53×10^{-7} in Eq. (16a). The effect of reducing k_d by a factor of 2.5 are shown in Fig. 7, where, for the sake of comparison, the reference case and the case for a 2.5 times *increase* in the value of k_d are also shown. The variation of the particle temperature and the particle mass (due to devolatilization and char burnout) are

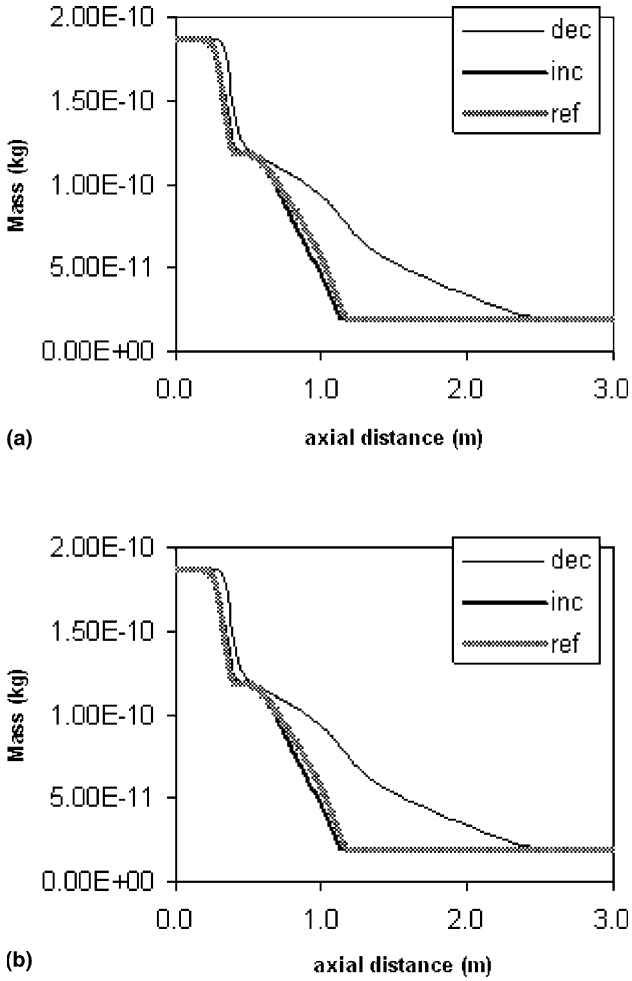

Fig. 7. Computed variation with axial position of (a) particle mass and (b) particle temperature for the reference case and for a decrease/increase in the oxygen diffusion rate by a factor of 2.5.

shown along the length of the furnace. The particle mass variation with length has four distinct phases: (i) the initial heating up stage where the mass does not change, (ii) the rapid devolatilization stage its mass decreases rapidly, (iii) the slower char burnout stage and (iv) the heating or cooling stage of the particle containing only ash. The effect of changing the oxygen diffusion rate for char burnout has a significant effect only on the third stage. Reducing the oxygen diffusion rate slows down the char burnout rate while increasing it marginally increases it. Examination of the particle temperature variation (Fig. 7a) shows that this has a strong effect on the peak particle temperature. In all the cases, the peak temperature occurs in the char burnout stage (see Fig. 7b). When the oxygen diffusion rate is increased, the faster burnout rate increases the maximum temperature to nearly 3000 K while with the decreased diffusion rate, the peak particle temperature is about 1000 K less. The peak gas temperatures also occur later in the furnace in the latter case although the peak value is nearly unchanged. The gas outlet temperatures are nearly the same.

These results show once again that the overall furnace parameters are dependent on the heat transfer characteristics rather than on the combustion characteristics. The presence of excess ash and the consequent decrease in oxygen diffusion rate may lead to substantial reduction in char combustion without significantly affecting the overall combustion parameters. Similar insensitivity of the peak and outlet temperatures to the increase in ash content has been reported by Kurose et al. [5] when investigating combustion of coals with ash content in the range of 36–53%.

3.5. Effect of radiative properties of the media

Another important effect of increase in ash content on the coal combustion is the change in the thermal and radiative properties of the coal and the gas inside the furnace. Sarofim et al. [11] found that the mineral matter increases the emissivity by an amount, which depends on the composition of ash and temperature. Also, increased ash content may result in increased thickness of the slag, which, since it contains the mineral matter of the ash, may increase the wall emissivity. Finally, increased thickness of the slag will also increase the temperature drop across the slag [18] and since the inside temperature is fixed, the wall temperature will increase. These effects are investigated individually as well as together in the following way:

The effect of radiative properties of coal and wall is analyzed by increasing the furnace wall temperature and its emissivity from 400 K to 600 K and from 0.2 to 0.25, respectively and as well as increasing both together. Calculations were also performed by increasing the emissivity of the char and the absorption coefficient of the gas from 0.6 to 0.75 and from 0.5 to 0.6 m^{-1}, respectively and as well as together. The effect of these changes, namely,

- Increasing char emissivity from 0.6 to 0.75
- Increasing gas absorption coefficient from 0.5 to 0.6 m^{-1}
- Increasing both simultaneously
- Increasing wall emissivity from 0.2 to 0.25
- Increasing wall temperature from 400 K to 600 K
- Increasing both the wall conditions simultaneously

are summarized in Tables 7 and 8. In all the cases, the temperature contours were found to be roughly similar and the values were largely unchanged. Increasing the wall emissivity reduces the peak temperature (as the radiative heat transfer is more) resulting in a reduced flue gas temperature. The reverse trend is obtained with

Table 7
Peak temperature, outlet temperature and predicted thermal output for different radiative properties of coal and gas

Emissivity of		Peak temperature (K)	Outlet temperature (K)	Thermal output (MW)
Char	Gas			
0.6	0.5	1956	1060	3.275
0.75	0.5	2010	1082	3.389
0.6	0.6	1990	1077	3.4
0.75	0.6	1966	1076	3.4

Table 8
Predicted peak and outlet temperatures for different wall conditions

Wall conditions		Peak temperature (K)	Outlet temperature (K)
Emissivity	Temperature (K)		
0.2	400	1956	1060
0.2	600	1963	1093
0.25	400	1927	1011
0.25	600	1937	1044

the increased wall temperature as this decreases the heat lost to the surroundings. When both the emissivities of the media and the wall parameters are increased simultaneously, the net effect on the temporal and axial variation of the particle temperature, mass of volatile and char release was found to be negligible as the two effects cancelled out each other leaving the overall parameters relatively unchanged.

4. Conclusion

The above set of calculations reiterates the complexity of the coal combustion phenomena. As far as the effect of increased ash content is considered, the present calculations show that effect of enhanced char reactivity is negligible whereas reduced oxygen diffusion rates due to a thicker ash layer may result in significant reduction in char oxidation rates as this is the governing rate for char combustion. The global parameters such as the peak temperature and the flue gas temperature remain relatively insensitive to the presence of high ash content. These results are consistent with the experimental observations of Kurose et al. [5].

The present calculations are based on a combustion model which is essentially built on an ash-free basis. The effects considered here, for example, those described by Smoot [14], are not directly based on investigations of the *amount* of ash in the coal. Such studies are really necessary to investigate, more fundamentally, the real effect, if any, of ash content on the combustion characteristics in a typical furnace.

Acknowledgement

The calculations reported here have been performed at the CFD Centre, IIT-Madras, India.

References

[1] F.C. Lockwood, A.P. Salooja, S.A. Syed, A prediction method for coal fired furnaces, Combust. Flame 38 (1980) 1–15.
[2] J.S. Truelove, Prediction of the near burner flow and combustion in swirling pulverized-coal flames, in: 21st Symposium (International) on Combustion, The Combustion Institute Pittsburgh, 1986, pp. 275–284.
[3] B.M. Visser, Mathematical modelling of swirling pulverized coal flames. Dissertation, Technische Universiteit Delft, The Netherlands, 1991.
[4] R. Weber, A.A.F. Peters, P.P. Breithaupt, B.M. Visser, Mathematical modeling of swirling flames of pulverized coal: What can combustion engineers expect from modeling, J. Fluids Engvol. 117 (1995) 289–297.
[5] R. Kurose, M. Ikeda, H. Makino, Combustion characteristics of high ash coal in pulverized coal combustion, J. Fuel 80 (2001) 1447–1455.
[6] E.E. Khalil, Modeling of Furnaces and Combustors, Abacus Press, TunbridgeWells, Kent, UK, 1982.
[7] F.A. Williams, Combustion Theory, second ed., Benjamin Cummings Publishing, Menlo Park, CA, USA, 1985.
[8] C.J. Lawn, Principles of combustion engineering for boilers, in: C.J. Lawn (Ed.), Combustion Treatise, Academic Press, 1987.
[9] J. Warnatz, U. Mass, R.W. Dibble, Combustion, Springer-Verlag, Berlin, Germany, 1996.
[10] J.H. Ferziger, M. Peric, Computational Methods for Fluid Dynamics, Springer, New York, USA, 1999.
[11] A.F. Sarofim, J.B. Howard, H. Kobayashi, Coal devolatilisation at high temperatures, in: 18th Symposium (International) on Combustion, The Combustion Institute, Pittsburgh, 1977, pp. 411– 425.
[12] S. Saxena, A. Rehmat, A mathemaical model for char combustion in a fluidized bed, in: Proceedings of the 6th International Conference on Fluidized Bed Combustion, vol. 3, 1980, pp. 1138–1149.
[13] I.K. Puri, Environmental Implications of Combustion Processes, in: I.K. Puri (Ed.), CRC Press, Boca Raton, FL, USA, 1993.
[14] L.D. Smoot, Fundamentals of Coal Combustion, Elsevier, The Netherlands, 1993.
[15] R.B. Bird, W.E. Stewart, E.N. Lightfoot, Transport Phenomena, Wiley, New York, USA, 1960.
[16] O. Levenspiel, Chemical Reaction Engineering, second ed., John Wiley and Sons, New York, USA, 1972.

[17] D.A. Libby, F.A. Williams, Turbulent Reacting Flows, Springer-Verlag, Berlin, Germany, 1980.
[18] T.F. Wall, The combustion of coal as pulverized fuel through swirl burners, in: C.J. Lawn (Ed.), Principles of Combustion Engineering for Boilers, Combustion Treatise, Academic Press, 1987 (Chapter 3).
[19] S. Badzioch, P.G.W. Hawksley, Kinetics of thermal decomposition of pulverized coal particles, Ind. Chem. Process Des. Develop. 9 (1970) 521–530.
[20] D.W. Field, B.B. Gill, P.G.W. Hawksley, The Combustion of Pulverized Coal, British Coal Utilization Research Association, Leatherhead, Surrey, UK, 1967.
[21] R. Viskanta, M.P. Menguc, Radiation heat transfer in combustion systems, Prog. Energy Combust. Sci. 13 (1987) 97–160.
[22] Z.U.A. Warsi, Fluid Dynamics: Theoretical and Computational Approaches, CRC Press, Boca Raton, FL, USA, 1993.
[23] P. Hutchinson, G.F. Hewitt, A.E. Dukler, Deposition of liquid or solid dispersions from turbulent gas streams: a stochastic model, Chem. Eng. Sci. 26 (1971) 419–439.